The variability of California summertime marine stratus: Impacts on surface air temperatures

Sam F. Iacobellis[1] and Daniel R. Cayan[1,2]

Received 23 February 2013; revised 10 July 2013; accepted 12 July 2013.

[1] This study investigates the variability of clouds, primarily marine stratus clouds, and how they are associated with surface temperature anomalies over California, especially along the coastal margin. We focus on the summer months of June to September when marine stratus are the dominant cloud type. Data used include satellite cloud reflectivity (cloud albedo) measurements, hourly surface observations of cloud cover and air temperature at coastal airports, and observed values of daily surface temperature at stations throughout California and Nevada. Much of the anomalous variability of summer clouds is organized over regional patterns that affect considerable portions of the coast, often extend hundreds of kilometers to the west and southwest over the North Pacific, and are bounded to the east by coastal mountains. The occurrence of marine stratus is positively correlated with both the strength and height of the thermal inversion that caps the marine boundary layer, with inversion base height being a key factor in determining their inland penetration. Cloud cover is strongly associated with surface temperature variations. In general, increased presence of cloud (higher cloud albedo) produces cooler daytime temperatures and warmer nighttime temperatures. Summer daytime temperature fluctuations associated with cloud cover variations typically exceed 1°C. The inversion-cloud albedo-temperature associations that occur at daily timescales are also found at seasonal timescales.

Citation: Iacobellis, S. F., and D. R. Cayan (2013), The variability of California summertime marine stratus: Impacts on surface air temperatures, *J. Geophys. Res. Atmos.*, *118*, doi:10.1002/jgrd.50652.

1. Introduction

[2] Marine stratus and stratocumulus clouds (hereafter referred to simply as marine stratus) cover more than 20% of the world's ocean surface [*Wood*, 2012] and play a critical role in the surface radiation budget on spatial scales ranging from local to global [*Randall et al.*, 1984]. Along the California coast, marine stratus are a very common feature, forming through the interaction between high pressure aloft and the cool marine boundary layer. The North Pacific High (i.e., subtropical high pressure formed in the descending branch of the Hadley Cell) is a dominant feature that affects California during the summer months. Descending air aloft within the high pressure cell is relatively warm and dry due to adiabatic compression. Summer ocean temperatures in the eastern boundary current offshore of California are relatively cool. As a result, the air directly over the marine surface is relatively cool and moist. A temperature inversion (defined as region where temperature increases with height) forms where the warm descending air aloft meets the cool air of the marine boundary layer.

[3] The inversion caps the marine boundary layer, preventing the cool moist marine air from mixing with the warm dry air above. As the cool moist air in the boundary layer mixes upward, the relative humidity often reaches saturation allowing stratus clouds to form just below the base of the temperature inversion [*Petterssen*, 1938; *Lilly*, 1968; and *Leipper*, 1994]. Once formed, cloud top radiative cooling is primarily responsible for the maintenance of the stratus clouds [*Lilly*, 1968; *Klein and Hartmann*, 1993; *Koracin et al.*, 2005] by driving convection within the marine boundary layer and maintaining the temperature gradient of the inversion layer [*Wood*, 2012]. Since the temperature inversion is a nearly constant summertime feature [*Iacobellis et al.*, 2009], these low-level marine stratus clouds that form just under the inversion are also a persistent feature alongshore and offshore of the California coastline reinforcing the inversion during these months.

[4] Figure 1 shows the climatological monthly means of low cloud coverage at 18Z (10 A.M. PST) based on 25 years (July 1983 to June 2008) of data from the International Satellite Cloud Climatology Project (ISCCP) D2 dataset [*Rossow et al.*, 1996]. The data are presented as a ratio of low cloud cover to total cloud cover, where low clouds are defined as having a cloud top pressure below the 680 hPa level. Low-level clouds are present throughout the year over California coastal waters and are the dominant cloud type, more than 50% and often more than 80% of all clouds, during

[1]Scripps Institution of Oceanography, University of California, San Diego, La Jolla, California, USA.
[2]U.S. Geological Survey, La Jolla, California, USA.

Corresponding author: S. F. Iacobellis, Scripps Institution of Oceanography, University of California, San Diego, 9500 Gilman Dr., La Jolla, CA 92093-0224, USA. (siacobellis@ucsd.edu)

©2013. American Geophysical Union. All Rights Reserved.
2169-897X/13/10.1002/jgrd.50652

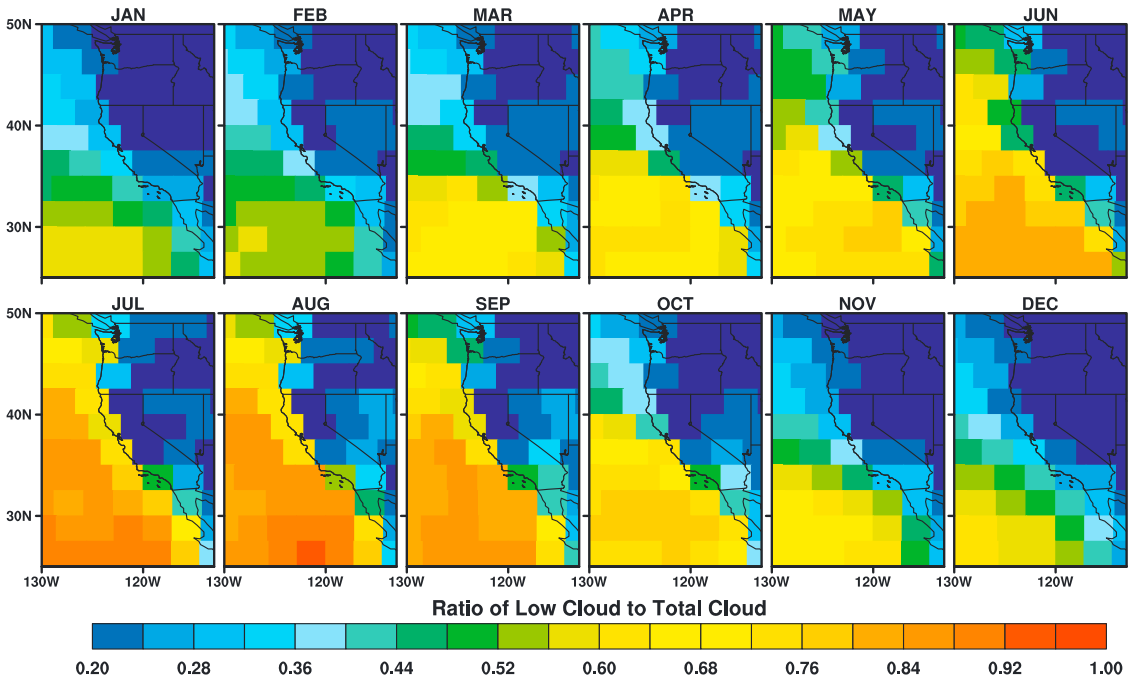

Figure 1. Ratio of low cloud cover to total cloud cover at 18Z by month based on 25 years (July 1983 to June 2008) ISCCP D2 data.

the summer months of June through September. These results are consistent with earlier studies that found maximum marine stratus amount during summer months using both surface-based [*Klein and Hartmann*, 1993] and satellite data [*Lin et al.*, 2009].

[5] Clouds impact surface temperature through daytime cooling from their reflection of incoming solar radiation and through nighttime warming from their downwelling infrared radiation (IR). It has been recognized [*Hartmann et al.*, 1992; *Klein and Hartmann*, 1993] that for low optically thick clouds such as marine stratus, the reflection of solar dominates over their downwelling IR radiation component, so the presence of these clouds tends to cool the surface. While marine stratus clouds are generally found over water [*Klein and Hartmann*, 1993], they often pervade the coastal margin and can thus impact land surface temperatures as well.

[6] Surface temperature in the Western United States contains anomalous variability from daily to multidecadal timescales [*Namias* 1978; *Alfaro et al.*, 2006]. Along the California coast, cloudiness varies seasonally but also exhibits anomalous fluctuations on timescales from synoptic events to decades [*Filonczuk et al.*, 1995; *Johnstone and Dawson*, 2010]. It is well known that there is a marine influence that affects summer temperature anomalies along the California coast [e.g., *Van den Dool and Nap*, 1985; *Alfaro et al.*, 2006; *Lebassi et al.*, 2009]. This linkage was demonstrated by *Johnstone and Dawson* [2010] who showed that the summertime fog frequency along the Northern California coastline increases as the gradient from coastal to inland temperature increases. They suggest that this association is due to year-to-year variability of subsidence, inversion conditions, and upwelling, processes that are largely controlled, jointly, by regional- to large-scale circulation variability. *Koracin et al.* [2005] constructed Lagrangian trajectories to study the life cycle of sea fog offshore of California. They found that local processes, including cloud top radiative cooling, were sufficiently strong to produce cooling within the marine layer despite increasing sea surface temperature (SST) (and surface fluxes) along the trajectory. This indicates that cloud top cooling and the resulting mixing through the boundary layer could play a significant role in coastal summer temperature anomalies. However, the direct linkage between clouds and temperatures has not been comprehensively investigated.

[7] The presence of marine stratus and their attendant effects on surface temperatures has many implications. *Gershunov et al.* [2009] show the absence of marine stratus along the California margin during heat waves can dramatically increase their coastal influence and in some cases have heightened human mortality rates in California coastal cities. The frequency and associated reflection of solar radiation by marine stratus may also have important consequences for the generation of solar energy [*Mathiesen et al.*, 2013]. Marine stratus also impact the growth of many endemic species when condensation from fog droplets provides an important source of moisture during the summer months when precipitation is infrequent [*Fischer et al.*, 2008; *Williams et al.*, 2008]. Fisheries and aquaculture may also be affected as water temperatures in lakes and streams can be sensitive to variability in marine stratus frequency [*Madej et al.*, 2006].

[8] Previous studies [e.g., *Klein and Hartmann*, 1993] investigated linkages between marine stratus variability and lower tropospheric stability (LTS) derived from reanalysis products, inferring that inversion strength plays a role in the formation and/or maintenance of these clouds. *Wood and Bretherton* [2006] derived an estimated inversion strength (EIS) using reanalysis data and found that marine stratus amount at a variety of global sites is more strongly correlated to their EIS parameter than LTS. *Lin et al.* [2009] also used

EIS to examine the seasonal variation of marine stratus amount. They found that the winter-to-summer variation in marine stratus amount is not so much due to differences in EIS but are more likely driven by the deepening-warming mechanism described by *Bretherton and Wyant* [1997] in which the cloud layer becomes decoupled from the marine boundary layer as the ratio of cloud top radiational cooling to surface heating decreased during winter. However, neither *Wood and Bretherton* [2006] nor *Lin et al.* [2009] examined the temporal variability of summertime marine stratus and possible relationships to EIS at a particular site.

[9] The present study examines the regional fluctuations of clouds, primarily marine stratus clouds, and how they are associated with daytime and nighttime temperature variations over California and Nevada, and especially along the California coastal margin. The focus is on the months of June through September when marine stratus clouds are the dominant cloud type along the California coastline. In contrast to many earlier studies, the present investigation utilizes high-resolution satellite measurements to determine the frequency and spatial extent of marine stratus and its impact on surface temperatures in this region.

[10] Section 2 describes the radiosonde and satellite data, along with the other data used in this study. Included in this section is a discussion of the method used to calculate cloud albedo and the assumptions and uncertainties in using this as a proxy for stratus cloud coverage. In section 3, we examine the relationship between temporal variations in marine stratus amount and different inversion characteristics, namely, inversion strength and inversion base height. We use values of cloud albedo, produced using visible satellite measurements with a 1 km spatial resolution, to determine the presence of marine stratus during the summer months when these clouds are the dominant cloud type. Inversion strength and base heights are determined using in situ measurements from operational radiosonde soundings at two locations in California allowing for a direct determination of the inversion strength and inversion base height. Section 4 is an analysis of the spatial features of cloud albedo (marine stratus). The spatial coherence and empirical orthogonal function (EOF) analysis of daily mean cloud albedo fields is derived to examine the typical spatial patterns of marine stratus coverage along the California coastline during the summer months. In section 5, the linkage between cloud albedo and surface temperatures at various locations in California is investigated. The fine spatial resolution of the satellite albedo measurements is well suited to study the response of surface temperatures to marine stratus along the topographically complex California coastal margin. Section 6 contains a discussion of the main findings of this study.

2. Data

[11] Albedo measurements were acquired from raw Geostationary Operational Environmental Satellite (GOES) data over the period 1996–2011, obtained from the National Oceanic and Atmospheric Administration's (NOAA) Comprehensive Large Array-data Stewardship System (CLASS) website at http://ww.nsof.class.noaa.gov and the University of Wisconsin Space Science and Engineering Center. This data set has a spatial resolution of approximately 1 km, and we employ samples at 30 min intervals throughout the daytime. The albedo is a measure of the reflectivity of the GOES pixel, defined as the ratio of reflected radiation from the surface to incident radiation upon it. In simple terms, as cloud cover increases, the albedo increases and the shortwave radiation reaching the surface decreases. In the coastal domain that is of greatest interest here, most of the variation in albedo values is caused by variations in clouds, but as noted below, the albedo may be modified by other factors such as vegetation and snow, water vapor, and aerosols. Values of albedo were computed from the raw GOES data using prelaunch and postlaunch calibration methods published by the NOAA's National Environmental Satellite, Data, and Information Service (NESDIS).

[12] For this study, measurements were obtained from GOES 9, 10, 11, and 15 satellites which were not equipped with onboard calibration for the visible imager. To account for the expected imager degradation, a postlaunch calibration is applied that makes use of onboard calibration systems available on other satellites such as Tropical Rainfall Measuring Mission and Moderate Resolution Imaging Spectroradiometer. In this study, we use the postlaunch calibration developed by NASA Langley (http://cloudsgate2.larc.nasa.gov/) for GOES 9 and 10 and the calibration developed at NESDIS (http://www.star.nesdis.noaa.gov/smcd/spb/fwu/homepage) for GOES 11 and 15. The postlaunch calibration has the additional benefit of significantly reducing the variability introduced by the changing GOES satellite systems [*Wu and Sun*, 2005].

[13] For each month and hour, a clear sky albedo value was determined for each pixel by sorting the albedos from all images for that month and hour and selecting the lowest albedo as the clear sky albedo. For example, clear sky albedos for April 2002 at 16Z were calculated by examining all images taken at this hour during the month (~30 images) and selecting the minimum albedo at each pixel as the clear sky albedo for that pixel. This method assumes that there will be at least one clear day during the month; however, variability of water vapor and other atmospheric constituents that may impact the albedo are not accounted for with this procedure. Separate clear sky albedos are calculated for each hour and each year because surface reflectance can be dependent on the angle of incoming solar radiation, the temporal and spatial extent of snow cover varies from year to year, and reflectance is dependent on vegetation that may also vary from year to year. The estimated cloud albedo is simply the measured albedo minus the clear sky albedo and is used as a proxy for cloudiness throughout this study. An estimate of the uncertainty in using this proxy is determined and discussed later in this section.

[14] Hourly observations of cloud cover, air temperature, and wind observed at the surface at several coastal airports in California (Figure 2) were obtained online from the NOAA's National Climatic Data Center (NCDC) Integrated Surface Data data set. Cloud observations include the portion of sky obscured by cloudiness along with the cloud ceiling height (i.e., cloud base height) and extend back to the 1950s at some airports. Cloud cover was originally reported in octas and then condensed into four categories: clear (no cloud cover), scattered (1/8 to 4/8 coverage), broken (5/8 to 7/8 coverage), or overcast (8/8 or 100% coverage). For calculating fractional cloud cover, a report of scattered and broken clouds were assigned a fractional coverage of 0.375

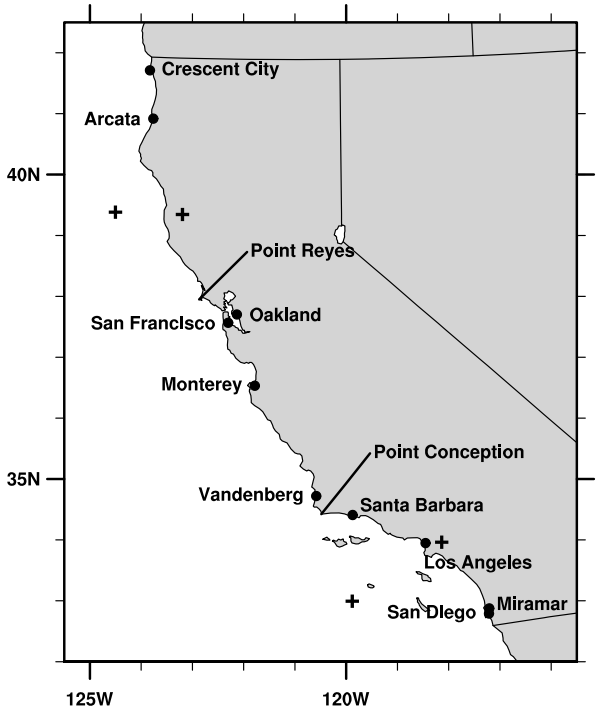

Figure 2. Map showing locations of airport observations, radiosonde sites, and coastal landmarks referred to in this study. The four crosses indicate pixel locations referred to in section 2.1.

and 0.75, respectively. Observations of cloud ceiling were only included for broken or overcast conditions and are provided in increments of 100 feet (30.5 m) above ground level. Cloud ceiling observations were converted to height above sea level using the elevation at each station. The cloud base measurement of the surface-observed cloud observation is an important element of the present study—while the satellite-based cloud albedo and its variability are a result of *all* clouds (and sometimes other factors), the surface-based observations that are derived here are formed by a subset of the cloud cover that has bases that are relatively close to the ground, thus isolating low cloud (stratus) cover.

[15] Observed values of daily minimum and maximum surface temperature (T_{MIN} and T_{MAX}, respectively) at many stations throughout California and Nevada were obtained from the NCDC Cooperative Observer (COOP) dataset [*National Climatic Data Center*, 2003]. COOP stations with record lengths a decade or longer were used, and, in the present version of the COOP dataset, the data runs through the year 2010.

[16] Radiosonde measurements provide a vertical profile of temperature, pressure, dew point, and horizontal winds, and are well suited to provide a measure of low-level temperature inversions. Radiosondes are routinely launched twice daily (currently at 0Z and 12Z) at locations throughout the United States including three sites in California: at San Diego Miramar Air Field (KNKX), Vandenberg (KVBG), and Oakland (KOAK). Radiosonde observations date from the 1950s to present and were obtained from archives maintained by the Earth System Research Laboratory of the NOAA [*Schwartz and Govett*, 1992]. Measurements are provided at standard pressure levels as well as significant levels defined by inflection points of temperature and/or dew point.

[17] The radiosonde measurements are used to determine if a temperature inversion is present and, if so, to estimate the strength and the height of the inversion base. Here, the inversion strength (DT_{INV}) is simply the temperature difference between the top and bottom of the inversion region, while the inversion base (Z_{BASE}) is the height above sea level of the bottom of the inversion. The temperature profile is examined between the surface and 700 hPa level for temperature inversions, defined to be present when a temperature at a given altitude in the sounding was warmer than the temperature at an altitude below it. In the case when more than one inversion is observed, the inversion having the largest value of DT_{INV} is used. Additional information on the processing of this data is found in *Iacobellis et al*. [2009].

[18] Downwelling solar radiation (DSR), at hourly intervals at the land surface, was obtained at weather stations maintained by the California Irrigation Management Information System (CIMIS). DSR is measured on a minute-by-minute basis and then stored as hourly means. Quality control is performed by CIMIS with questionable data flagged in the data files.

[19] A key question that bears on the present study is how well do GOES cloud albedo measurements represent summertime solar attenuation along California's coastal margin? To address this, daily June–September (JJAS) solar attenuation based on measurements at six coastal CIMIS sites was compared to colocated daily mean GOES cloud albedo. The six sites were chosen for their proximity to the coastline and a record length of at least 10 years. Excellent agreement, with correlations of 0.90 or greater, were found at all six locations justifying the use of GOES cloud albedo to simulate solar attenuation at coastal sites during summer months.

[20] Sea surface temperature (SST) was obtained from the NOAA Optimum Interpolation SST (OISST) V2 data set [*Reynolds et al*., 2002] available online at www.esrl.noaa.gov. This data set combines satellite and in situ measurements of SST and comes on a $1° \times 1°$ spatial grid and has a weekly temporal resolution. Linear interpolation was used to estimate daily values as needed.

[21] Geopotential heights were obtained from National Centers for Environmental Prediction (NCEP) Reanalysis 1 products [*Kalnay et al*., 1996]. The NCEP Reanalysis project assimilates available past observational data into a state-of-the-art atmospheric model to produce dynamically consistent data on a global grid with a horizontal resolution of 2.5° and 17 vertical pressure levels from 1948 to present at a 6 h resolution.

2.1. Cloud Albedo as a Proxy for Cloudiness

[22] Throughout this study, cloud albedo will be used as a proxy for cloudiness, where cloud albedo is simply the GOES measured top of atmosphere albedo minus the clear sky albedo. Day-to-day fluctuations in various atmospheric constituents other than clouds can impact the measured albedo and thus introduce some uncertainty in the use of this proxy.

[23] The clear sky albedo depends primarily on the surface albedo, atmospheric humidity, and aerosol concentration, where variations in the concentration of the later two

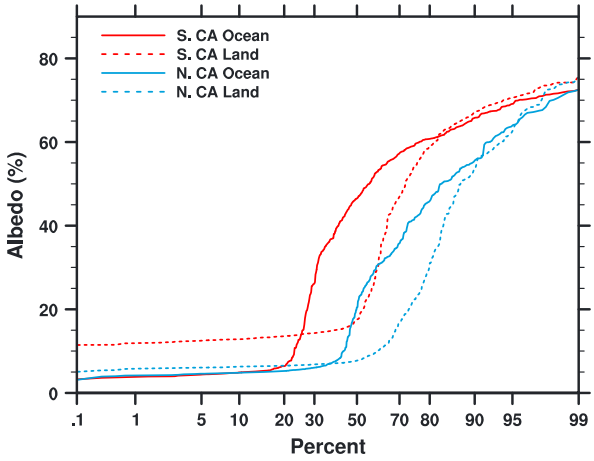

Figure 3. Cumulative distribution functions at four pixel locations based on 1700Z (9 A.M. LST) satellite images during June 1996–2011. The locations of the four pixels are shown in Figure 2.

constituents can lead to changes in atmospheric reflection (i.e., scattering) and absorption of solar radiation. While day-to-day changes in surface albedo are likely to be small along the coastal margin during summer months (i.e., no impacts from snow cover), daily variability in humidity and aerosol concentration could lead to uncertainty in the clear sky albedo.

[24] Numerical experiments were performed using the solar radiation parameterization from the NCAR CCM3 [*Briegleb*, 1992] to provide a first-order estimate of this uncertainty. This solar radiation scheme is well suited to this analysis, including the radiative impacts of clouds, water vapor, ozone, and aerosol concentrations. We implemented two sets of control runs of CCM3 using mean summertime temperature and humidity profiles determined from radiosonde data at Miramar. An aerosol profile was used that combined both continental and maritime background concentrations [*World Meteorological Organization*, 1983; *d'Almeida et al*., 1991] The overall aerosol optical depth was 0.20 which closely matches typical summertime values along the California coastline measured using the Multiangle Imaging Spectroradiometer spectral channel 2 (0.55 μm) on the NASA's Terra satellite (data available at www-misr.jpl.nasa.gov).

[25] The first set of control runs used clear (no clouds) conditions, while the second incorporated a single layer of cloud simulating marine stratus. The cloud was modeled with a geometric thickness of approximately 300 m, a liquid water content of 0.3 g m^{-3}, and a droplet radius of 10 μm, typical of summertime marine stratus [*Hess et al*., 1998]. The solar zenith angle was set to simulate a noontime midsummer day. Results from these two runs yielded top of atmosphere albedos of 9.3% (clear sky) and 42.6% (cloudy).

[26] The sensitivity of clear sky albedo to atmospheric humidity was estimated by increasing the precipitable water content (PWC) in the control runs (PWC = 2.4 cm) to the 90 percentile value (PWC = 3.5 cm) as measured by the Miramar radiosonde data. The PWC was varied by applying a constant factor to the specific humidity in each model layer being careful not to produce any supersaturated layers. This increase in atmospheric water vapor lead to an increase in the modeled clear sky albedo from 9.3% to 9.9%. The potential impact of changes in atmospheric aerosol concentration were estimated by doubling the aerosol optical thickness from 0.2 to 0.4. This increase in aerosol concentration leads to an increase in the modeled clear sky albedo from 9.3% to 11.4%.

[27] Based on these tests, the sensitivity of the clear sky albedo to variations in atmospheric humidity and aerosol concentration is estimated to be about 2%. This uncertainty is small compared to the reflectivity of marine stratus clouds that generally exceeds 30% [*Stephens*, 1978; *Rossow and Schiffer*, 1991; *Klein and Hartmann*, 1993] and is thus not expected to lead to significant errors in the identification of these clouds with the method used in this paper. Furthermore, as discussed later in this paper, cloud albedo variability is strongly correlated with both ground observer cloud cover and surface measurements of solar radiation.

[28] Aerosol concentration can also impact albedo through interactions with clouds, known as aerosol indirect effects [*Intergovernmental Panel on Climate Change*, 2007]. The first indirect effect occurs as an increase in aerosols causes an increase in droplet number concentration and a corresponding decrease in droplet size assuming the cloud water concentration is constant. Here we estimate the sensitivity of albedo by assuming a doubling of the droplet number concentration which would lead to a decrease in the effective droplet radius to 8 μm (compared to control value of 10 μm). This yields an increase in the modeled albedo (with cloud layer in place) from 42.6% to 47.0%. While this uncertainty is larger than that associated with the clear sky albedo, it is still relatively small compared to the typical reflectivity of marine stratus.

[29] A decrease in precipitation efficiency, leading to increases in cloud thickness and lifetime and thus more solar reflection, can also occur when cloud droplet size decreases and is known as the second indirect effect. Due to the more complex cloud microphysics, estimating the sensitivity of albedo to this effect is beyond the limitations of our simple modeling experiment. It is important to note that this simple analysis does not address the possible influence of aerosols and humidity in these relationships, such as changes in aerosol or humidity concentration with inversion strength. Additionally, our analysis has assumed no spatial variation in either humidity or aerosol concentration. *Wood* [2012] showed that cloud droplet concentration has a strong gradient along the California coastline which could conceivably impact comparisons of albedo over the coastal margin and nearby offshore waters. Implications of these potential "secondary" relationships are discussed in section 6.

[30] The uncertainty in clear sky albedo can also be estimated using an empirical approach, by examining the cumulative probability distribution of the GOES-observed albedo at a selected location. Figure 3 shows the cumulative probability distribution at four selected pixels (locations denoted by crosses in Figure 2) of 1700Z (9 A.M. local standard time (LST)) albedo during June 1996–2011 and is based on data from 480 individual images (albedo is only examined at a particular hour during a single month to minimize differences in solar zenith angle).

[31] Each distribution plotted in Figure 3 consists of two distinct regimes: (i) the observations which are confined to

a narrow range of slowly increasing albedo, which we assume represent clear sky conditions, and (ii) the observations which comprise a rapid albedo increase, which are assumed to consist of a range of increasingly cloudy conditions. The range of albedo values contained within the slowly varying portion of each distribution quantifies the variability of albedo during clear sky conditions and hence provides a data-informed estimate of the contributions of both humidity and aerosols to the albedo variability. This range presumably also includes changes in surface albedo, which are expected to be small, particularly for pixels over water. The variability of clear sky albedo, about 2–3% over the ocean pixels and about 4–5% over the land pixels, corresponds closely with values derived above using model-estimated solar radiation parameterization. Similar values were obtained with different times of days and different months within the JJAS period.

[32] In this study, we assume that any spatial variability of humidity and aerosols (e.g., difference between land and water values), as well as their impacts on albedo, is consistent through time and thus would be accounted for in the determination of clear sky albedo. Relationships between thermal inversion characteristics and the presence of marine stratus are examined in section 3.

3. Structure of California Marine Stratus Clouds

3.1. Seasonal Mean Cloud Albedo

[33] Figure 4a shows seasonal mean cloud albedo calculated for summer (JJAS) and winter (DJFM, December–March). These seasonal means were calculated using albedo values during the hours from 16Z to 00Z corresponding to 8 A.M. to 4 P.M. local standard time (LST). The diurnal structure of marine stratus clouds varies significantly from region to region along the California coast (not shown) as influenced by elevation, proximity to the coastline, and orientation of the coastline. To minimize noise caused by these variations, the daily mean albedo averaged over available daylight hours is used throughout this paper.

[34] The climatological mean albedo shows that during summer months (JJAS), there is often a very strong contrast in cloud albedo in the region of the California coastline. The strongest feature is the considerably higher mean values over the ocean, which is often cloudy, compared to the land, which is mostly cloud free. There is a fringe of intermediate albedo values along the coastal margin, where high cloudiness over the ocean transitions to low cloudiness inland. There is also structure on smaller regional scales, particularly over coastal plains and throughout the Southern California Bight (SCB). On average, the maximum cloud albedo is observed 10–50 km or more offshore of Central and Southern California

[35] An area of relatively high cloud albedo is observed over the ocean extending southward from approximately San Francisco Bay. South of Point Conception, the region of maximum cloud albedo is west of the Channel Islands with significantly lower cloud albedo values over the SCB.

[36] During winter months (DJFM), snow is often present at higher elevations, particularly in the northern half of the state and in the Sierra Nevada range. Thus, in these locations, satellite-measured albedo may be strongly affected by reflected radiation from snow. Accordingly, during winter months our analysis of satellite albedo is focused over the ocean and along the coastal margin where snow is rarely, if ever, present. Along the California coastline, cloud albedo generally increases from south to north and there are much smaller differences between offshore and onshore locations compared to summer months. Also, albedo values over the eastern North Pacific, from Point Reyes southward, are lower, because stratus clouds are less persistent in winter than in summer.

[37] The year to year variability of cloud albedo for summer and winter seasons is indicated in Figure 4b, where the standard deviation of cloud albedo is calculated using the 16 individual seasonal means from the years 1996–2011. For DJFM, individual seasonal means were calculated using contiguous months (e.g., the 1996 DJFM is December 1995 and January–March 1996). The spatial pattern of daily albedo variability, calculated from individual summer and winter days (not shown), resembles the pattern of variability of their respective seasonal means but is amplified due to the large day-to-day fluctuations.

[38] During summer, areas of highest year-to-year variability of cloud albedo are generally over the ocean with maximum values over the southern portion of the SCB. Higher variability is also noted over the Sierra Nevada mountains and is likely associated with daytime convective activity. Moderately high variability occurs over many of the coastal regions suggesting there is significant variability in the inland penetration of marine layer clouds from year to year.

[39] Compared to summer, there is much higher variability in cloud albedo along California's coastal regions during winter, indicative of the year-to-year changes in synoptic storm activity. During winter, minima in both cloud albedo mean and variability are noted over the desert regions of Southeastern California and Southern Nevada.

3.2. Thermal Inversions and Coastal Cloud Variations

[40] The presence of low-level temperature inversions over the California region is closely tied to coastal marine clouds [*Lilly*, 1968; *Pilie et al*., 1979] and by association would also be linked to coastal temperature variability. Low-level thermal inversions are nearly always present along the California coast during summer months but vary in their degree of development and structure.

[41] Stronger inversions limit entrainment at cloud top [*Rozendaal et al.*, 1995; *Wood and Bretherton*, 2006] and thus provide a barrier which generally increases the lifetime (and hence frequency) of marine stratus clouds [*Wood*, 2012]. The horizontal extent and duration of marine stratus clouds are also dependent on the height of the inversion base, because higher inversion base heights will generally allow thicker clouds to develop (assuming constant lifting condensation level). The liquid water path is usually assumed to increase as marine stratus becomes physically thicker [*Blaskovic et al.*, 1991; *Duynkerke and Hignett*, 1993] and thus would take longer to evaporate and dissipate. Importantly, as inversion base height increases, the inland penetration of these clouds increases, since higher clouds are less constrained by coastal topography.

[42] As a result, strong inversions and higher inversion base heights are associated with increased frequency of marine stratus clouds along the California coast. However, these two inversion characteristics are usually inversely related [*Wood*, 2012]. Figure 5 shows this inverse relationship in the seasonal

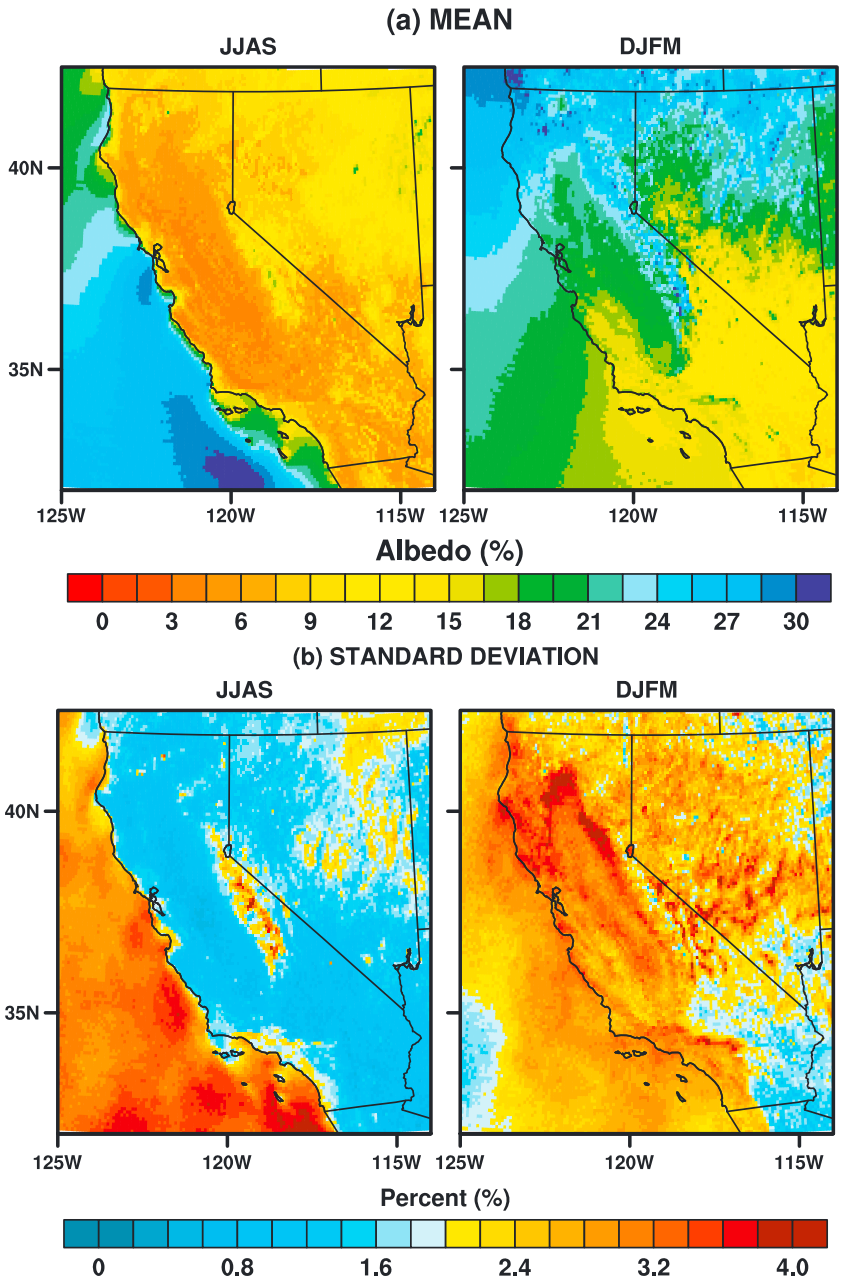

Figure 4. GOES-derived (a) long-term seasonal mean cloud albedo and (b) standard deviation of seasonal mean calculated during 1996–2011 period. Separate plots are shown for June–September (JJAS) and December–March (DJFM). Albedo means computed using values during hours 16–00Z (8 A.M. to 4 P.M. LST).

cycle of inversion strength and inversion base height derived from radiosonde profiles at Miramar, CA (near San Diego). As inversion strength increases during summer months, the inversion base height decreases. The summer to winter seasonal variation of inversion strength shown in Figure 5 is considerably larger than estimates presented by *Lin et al.* [2009] derived from North American Regional Reanalysis. Reasons for the difference in amplitude are that inversion strength shown in Figure 5 is based on land-based radiosonde measurements while those from *Lin et al.* [2009] are based upon a residual calculation of model variables along a transect extending over the Northeastern Pacific.

[43] Table 1 shows the linear correlation coefficients between time series of the mean JJAS values of inversion strength, inversion base height, cloud albedo, and daily temperature maximums at Monterey and San Diego during the 1996–2011 period. Significant negative correlations exist between inversion strength (DT_{INV}) and inversion base height (Z_{BASE}) at both locations. Significant negative correlations are also obtained (not shown) for monthly and daily means, and there are moderate to strong correlations between these inversion characteristics and either cloud albedo and daily maximum temperature. However, since inversion strength and inversion base heights are not completely

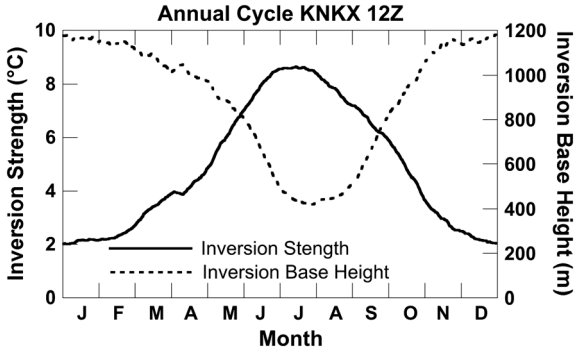

Figure 5. Annual cycle of inversion base height (dashed line) and inversion strength (solid line) derived from daily 12Z radiosonde profiles at Miramar/San Diego (KNKX) during 1960–2010 period. A 31 day running mean filter was applied to each curve.

independent (i.e., inversion strength depends in part on the height of the inversion), these correlations are ambiguous. Spearman rank correlation coefficients were also computed to test for the possibility of nonlinear monotonic relationships. The magnitude of the rank correlation coefficients was generally equal to or less than the linear coefficients with the lone exception being an increase from 0.53 (linear) to 0.65 (rank) between Z_{BASE} and T_{MAX} at San Diego.

[44] To better understand the individual contributions of these two inversion characteristics and marine stratus clouds, the following procedure was implemented. Correlations between GOES albedo and inversion strength were calculated only using days when the inversion base height was within 75 m of the monthly median value thereby limiting the impact of inversion base height variability on marine stratus. Similarly, only days when the inversion strength was within 0.6°C of the monthly median value were used to compute correlations between GOES albedo and inversion base height. These threshold values were chosen so that approximately 20% of available days (approximately 100 out of 500 available days per month based on 1996–2011 period) would be included in the computation.

[45] Figure 6a shows the correlations between daily values of 12Z (4 A.M. LST) inversion strength at Miramar (San Diego) and daily 16–20Z (8 A.M. to noon LST) mean GOES albedo during the month of July using only days when inversion base height was within 75 m of the monthly median. Significant positive correlations occur, but they are mostly confined to coastal waters extending westward about 100–200 km. Over coastal land, the correlation between inversion strength and albedo is generally negative and weak. Figure 6b shows correlations between 12Z inversion base height at Miramar and daily mean (16–20Z) albedo during July, using only days where the inversion strength was within 0.6°C of the monthly median. As with correlations with inversion strength, significant positive correlations occur over coastal waters and extending westward. However, significant positive correlations with inversion base height extend over much of the lower elevation coastal land regions of Southern California. Thus, while inversion strength is generally not a factor associated with the inland occurrence of marine stratus, the inversion base height is—higher base heights permit greater inland cloud cover. For example, if the inversion base height is low, the clouds that initially form over water would be prevented from extending over land by the coastal topography. In regions to the north, correlations of inversion strength and base height using available radiosonde measurements at Vandenberg and Oakland provide similar results that yield the same conclusion. We should note that there are regions with intermediate elevations which exhibit a nonlinear relationship between Z_{BASE} and albedo and that the linear correlation coefficient used here may actually underestimate the strength of this relationship.

4. Spatial Variability of Summer Cloud Albedo

4.1. Spatial Coherence

[46] Figure 7 indicates the spatial coherence of marine stratus clouds relative to San Francisco and San Diego during summer months (JJAS). These maps are cross correlations of monthly mean albedo at exposed coastal sites at San Francisco and San Diego with that at all other grid points.

[47] At both locations, marine stratus clouds are spatially coherent (as indicated by relatively strong correlations exceeding 0.5) at distances of hundreds of kilometers along the coast but confined to lower, coastal-connected elevations by higher terrain which rises above about 600 m. The patterns are very similar for monthly and daily (not shown) timescales although the magnitudes of the correlations are stronger for monthly means, which may result from averaging out smaller-scale synoptic influences and also the fact that there are only 64 months compared to 1920 days. The broad spatial features of these cross correlations are in qualitative agreement to correlations *Johnstone and Dawson* [2010] found between a multistation Northern California fog index and sea level pressure.

[48] For San Francisco, the strong correlations extend about equal distances up and down the coast, whereas for San Diego, they extend a considerably larger distance southward compared to northward. Seaward from the coastline, the strong spatial coherence at each location extends out into the Pacific in a south-southwest direction, indicating the stronger association of marine stratus toward the south than to the west (or the northwest).

[49] Within the cross-correlation maps at both San Diego and San Francisco, a strong transition occurs at Point Conception, where the coastline to the north is oriented

Table 1. Correlations Between Temperature, Cloud Albedo, and Inversion Properties[a]

	DT_{INV} versus Z_{BASE}	DT_{INV} versus Albedo	DT_{INV} versus T_{MAX}	Z_{BASE} versus Albedo	Z_{BASE} versus T_{MAX}	T_{MAX} versus Albedo
Oakland/ Monterey	**−0.87**	0.36	−0.49	−0.10	0.17	**−0.82**
Miramar/ San Diego	**−0.68**	**0.63**	**−0.73**	−0.32	**0.53**	**−0.50**

[a]Correlations calculated using yearly JJAS mean values during 1996–2011 period. Correlations significant at the 95% confidence level are displayed in bold font. Inversion magnitude (DT_{INV}) and inversion base height (Z_{BASE}) are derived from radiosonde measurements at Oakland and Miramar (San Diego). Cloud albedo and daily temperature maximum (T_{MAX}) are based on measurements at nearby coastal airports (Monterey Airport and San Diego Lindbergh Field).

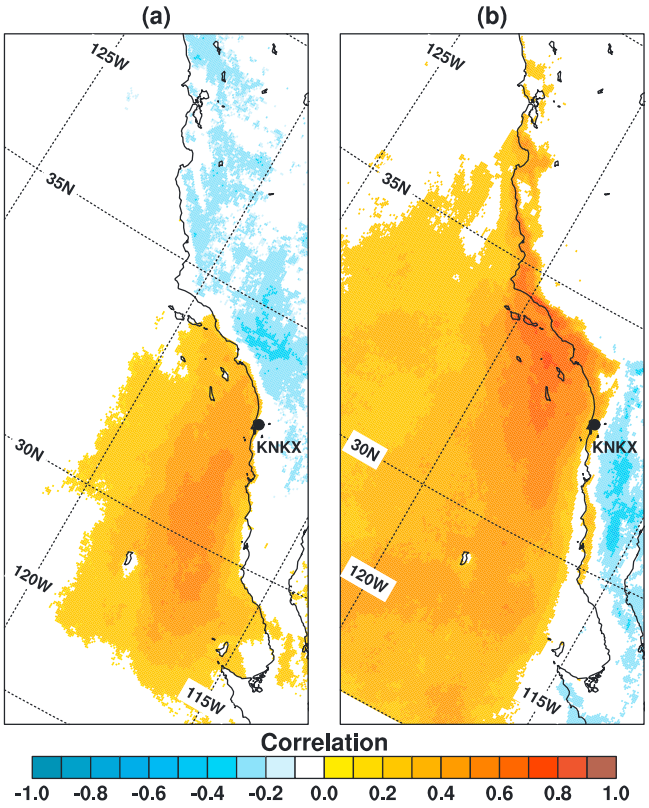

Figure 6. Maps showing correlation of GOES-derived daily mean albedo (16–20Z) at each 1 km^2 cell over the mapped domain versus the (a) 12Z inversion strength (DT_{INV}) and (b) 12Z inversion base height (Z_{BASE}) at Miramar (KNKX) during 1996–2011 for months of July. Only correlations significant at the 95% level are shown. Correlations of albedo versus inversion strength (inversion base height) were computed using days with a limited range of inversion base height (inversion strength). See text for details of procedure.

roughly south to north and the coastline to the south takes an abrupt change to the southwest. For the San Diego case, the strong positive correlations along the coast extend northward up to Point Conception but decrease abruptly north of this location. Likewise, for San Francisco, strong correlations extend southward to Point Conception but diminish to the south of this point. This suggests that large-scale features related to the formation of marine stratus may differ for the two locations. This possibility is further addressed using rotated empirical orthogonal functions in the next section.

[50] Figure 7b presents a higher resolution view showing the cross correlation of daily mean albedo at San Francisco and San Diego with that at other locations in the region, indicating the regional coherence in cloud cover fluctuations, and also the strong role that coastal land features play in determining the inland penetration of marine stratus cloud anomalies. At both locations, the regions of high correlations are sharply bounded by coastal topographic features.

[51] At San Francisco, regions of high spatial coherence extend into the Sonoma and Napa Valleys to the north and into the Salinas Valley to the south. In Southern California, spatially coherent clouds relative to San Diego extend into the Los Angeles region and continue northward to Point Conception. In both Northern and Southern California it is clear that the inland extent of marine layer clouds is limited by the coastal topography. In other words, marine stratus clouds extend inland only until they meet land with an elevation as high as the cloud top height. Thus, the inversion base height controls the vertical extent of marine stratus, and this, together with coastal topography, controls the inland penetration of these clouds.

[52] *Iacobellis et al*. [2009] showed that the strength and height of the overlying thermal inversion have relatively large horizontal length scales on the order of hundreds of kilometers. This is also indirectly evident from Figure 7b since the vertical extent of marine stratus is determined in large part by the height of the inversion base. Additionally, *Iacobellis et al*. [2009] found that inversion properties were strongly linked to large-scale circulation features, which appear to also link to the marine stratus variability.

4.2. Rotated EOF Analysis of Daily Mean Albedo

[53] The correlations in Figure 7 indicate that marine stratus clouds vary coherently over hundreds of kilometers along the California coastline. Here, an EOF analysis is used to elucidate the temporal and spatial characteristics of these patterns. The analyses use summer daily mean anomalies, seasonal cycle calculated and removed at each 1 km grid point, of GOES-derived cloud albedo over the region 32°N–43°N, 114°W–128°W. The series of JJAS daily data from 1996 to 2011 provided a total of 1952 daily maps. Once computed, the leading six EOFs (containing 68% of the total

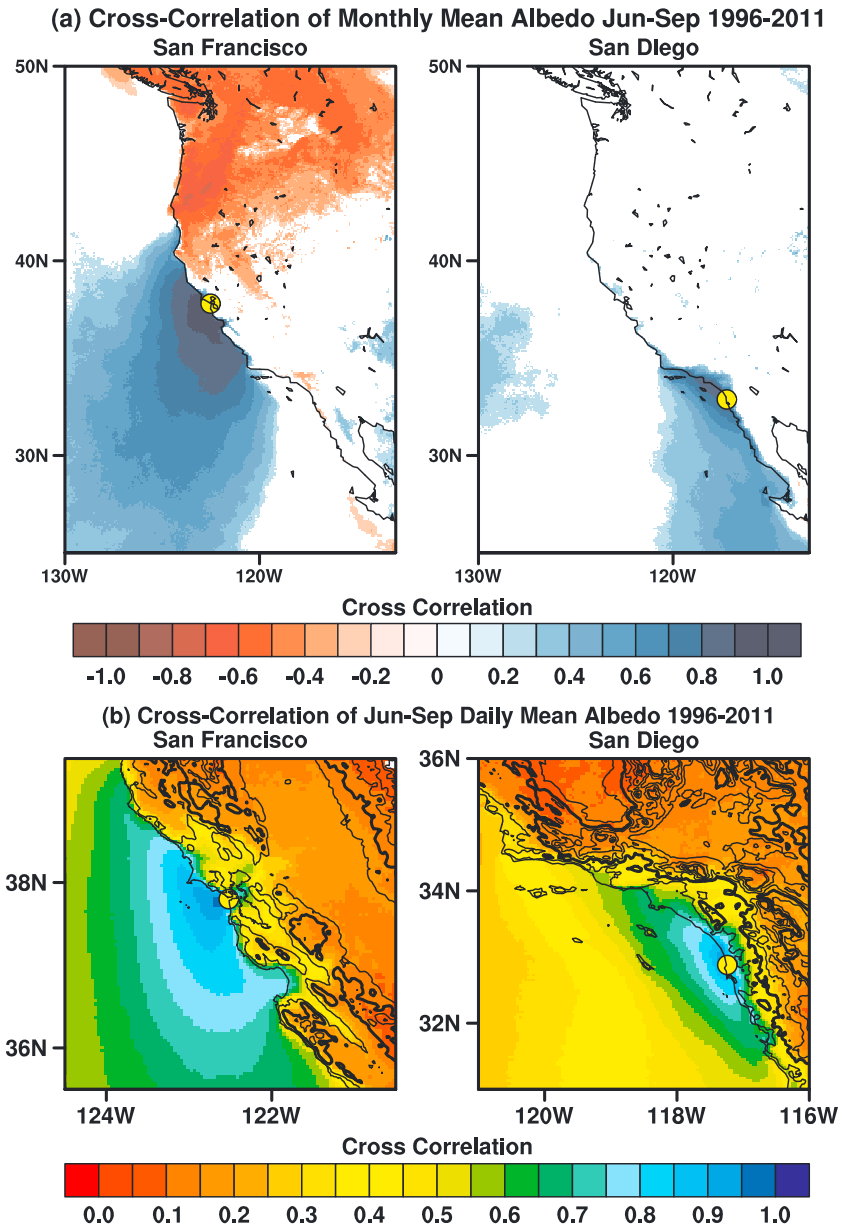

Figure 7. Cross correlation of (a) monthly mean albedo at San Francisco and San Diego with that at all other locations during June–September 1996–2011. (b) A close up view of the spatial coherence of daily mean albedo with elevation contours at 400 m intervals starting at 200 m (thick black contour line is 600 m). Monthly and daily means computed using albedo values during hours of 16–00Z (8 A.M. to 4 P. M. LST). Only correlations significant at the 95% confidence level are displayed.

variance) were then "rotated" using Kaiser row normalization and the varimax criterion [*Kaiser*, 1958] to obtain spatial patterns that are more suitable for physical interpretation than their unrotated counterparts [*Horel*, 1981; *Richman*, 1986]. The rotated principal components are no longer spatially orthogonal, but they do retain temporal orthogonality.

[54] Based on a series of trials, six EOFs were rotated to obtain the rotated EOFs (REOFs). In these trials, the number of original EOFs to be rotated was varied from 6 to 12, but all of these produced leading rotated EOF (REOF) patterns that were very similar with only minor differences in the principal component time series and amount of variance explained.

[55] Figure 8 shows the four leading REOF patterns of anomalous daily mean cloud albedo, which together explain 56% of the anomalous albedo variability. Three of the four patterns display a high contrast along a significant portion of the California coastline, with the dominant action occurring in area from the coast westward. These first three REOFs are indicative of the variability of marine stratus clouds. Also included in Figure 8 are histograms showing the monthly frequency of each REOF, where frequency is based on the number of days that the principal component (PC) exceeded the 90 percentile value. For the phase of the patterns shown for REOFs 1, 2, and 3 shown in Figure 8, a

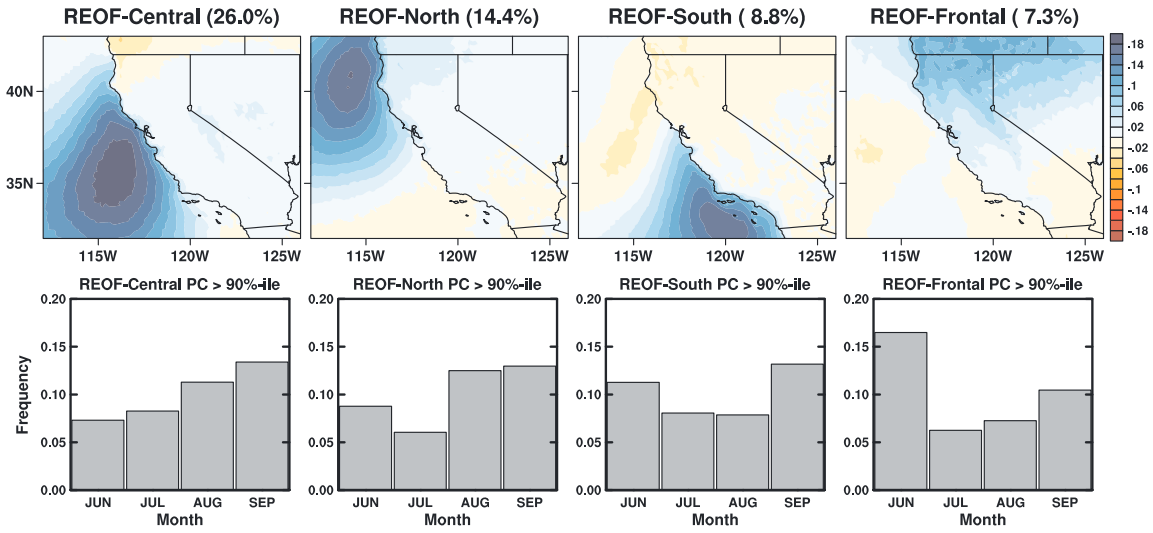

Figure 8. The four leading REOF patterns of anomalous daily mean cloud albedo along with the amount of variance explained. Histograms show the frequency of occurrence of the positive phase of each REOF by month, where frequency is based on the number of days that the principal component (PC) exceeded the 90 percentile value.

90% or higher PC value indicates a day with greater cloudiness over the oceanic portion of the domain.

[56] REOF1, which is called REOF-Central for ease of identification, represents a pattern of anomalous oceanic cloud cover variation along nearly the entire length of the California coast and explains more than 25% of the total variance. In its positive phase, REOF-Central represents positive cloud albedo values extending along most of the California coastline and westward several hundreds of kilometers into the Pacific. The albedo is markedly lower over land and the extreme northern and southern portion of the California coastal region. The positive phase of REOF-Central has a peak frequency during September.

[57] REOFs 2 and 3 are patterns of strong anomalous albedo values over the Northern (REOF-North) and Southern (REOF-South) California coastline, respectively. Similar to REOF-Central, there is a strong contrast along the coastline with generally low values over most land regions. When in their positive phase, the region of high albedo values extends a small distance inland onto the coastal margin along portions of the Northern California and extreme Southern California coastline. The positive phase of REOF-North occurs more frequently in August and September than in June and July, while the positive phase of REOF-South occurs more frequently in June and September than in July and August. The large-scale structure of the REOFs is further evidence that anomalous summertime marine stratus frequency along the California coast is associated with large-scale circulation variability. The broad patterns found in these first three REOFs reflect the spatial structure of correlations between annual summertime Northern California fog frequency and sea level pressure described by *Johnstone and Dawson* [2010].

[58] In contrast to the first three REOFs, REOF 4 (called REOF-Frontal) is most active over the North American continent and does not exhibit a distinctly marine cloud variability signature. The positive phase of this pattern (i.e., large positive albedo values over the northern portion of the region) is likely associated with synoptic-scale low-pressure systems which in general would not produce clouds preferentially over land or water. The positive phase of REOF-Frontal occurs most strongly in June, considerably less frequently in July and August and somewhat strongly in September.

[59] An important characteristic of the REOF patterns is their persistence, e.g., how long might a particular pattern of marine stratus endure. The persistence of the REOF cloud albedo patterns was measured by determining the time lag at which the principal component time series becomes decorrelated, where decorrelation occurs when the correlation falls below a value of e^{-1}. To make this determination, autocorrelations of each principal component time series were calculated using time lags varying from integral values of 0 to 5 days. Linear interpolation was then used to estimate a decorrelation time in fractional days. Of these four patterns, REOF-Central and REOF-South were the most persistent with decorrelation times of 1.8 and 1.6 days, respectively. A decorrelation time of 1.3 days was estimated for both REOF-North and REOF-Frontal. These decorrelation times are larger than the 0.7 to 1.2 days calculated from principal component time series of the four leading REOF cloud albedo patterns during winter (DJFM) months (not shown). This indicates that the summer cloud patterns dominated by marine stratus are somewhat more persistent than winter cloud patterns, which are more likely associated with transient synoptic systems.

[60] The linkage between low-level temperature inversion characteristics and the occurrence of these REOF patterns is examined by calculating the mean inversion strength and inversion base height during days that strongly resemble the first four REOF patterns. In this study, a day in which the principal component of an REOF exceeds its 90 percentile value while the remaining three leading REOF PCs lie between the 10 and 90 percentile values is defined to strongly resemble the REOF pattern (referred to as strong REOF X days, where X = Central, North, South, or Frontal). This method leads to a composite containing between 78 and

Table 2. Mean Inversion Strength and Base Height Anomalies (Means) During Strong REOF Days[a]

	Inversion Strength (°C)				Inversion Base Height (m)			
	REOF1 Central	REOF2 North	REOF3 South	REOF4 Frontal	REOF1 Central	REOF2 North	REOF3 South	REOF4 Frontal
Oakland	**2.9**	0.2	**2.1**	**−3.8**	−6	**155**	**−121**	**379**
	(13.2)	(10.2)	**(11.7)**	**(5.6)**	(427)	**(595)**	**(323)**	**(828)**
San Diego	0.7	0.1	**1.1**	**−1.6**	−25	56	**105**	**225**
	(9.5)	(8.8)	**(9.7)**	**(6.9)**	(352)	(441)	**(527)**	**(668)**

[a]Student *t* scores were calculated and used to determine significance. Values shown in bold font are significant at the 95% level.

133 days, depending on the REOF pattern. For the phase of the REOF patterns shown in Figure 8, days that strongly resemble REOF-Central, REOF-North, and REOF-South represent days with marine layer clouds along a significant portion of the California coastline.

[61] Mean anomaly values of inversion strength and inversion base height derived from radiosonde measurements at Oakland and Miramar (San Diego) during strong REOF days are shown in Table 2 (radiosonde measurements from Vandenberg were not included due to missing data). Days with widespread marine stratus clouds (strong positive REOF-Central, REOF-North, and REOF-South days) are associated with positive inversion strength anomalies at both radiosonde sites with values significant at the 95% level occurring at Oakland for REOF-Central and REOF-South and at San Diego for REOF-South. However, for days with widespread stratus, anomalies of inversion base height are not consistently associated with the first three REOF patterns. During strong positive REOF-North days, when cloudiness offshore of Central and Northern California is enhanced, significantly higher inversion base heights are found at Oakland, and during strong positive REOF-South days, when cloudiness offshore of Southern California is enhanced, significantly higher inversion base heights are found at San Diego. The REOF-North and REOF-South base height associations reinforce the effect of stronger inversion strength on days when there is heavy offshore marine stratus cover that penetrates onto the coastal land margin. In contrast, strong positive REOF-Central days appear only to associate with significant changes in inversion strength, having inversion base heights close to normal or below normal at Oakland and San Diego. For REOF-Frontal cases when cloudiness is high, the composite inversion base height is high in Oakland and San Diego, but the composite inversion strength anomaly is negative (weaker inversions), opposite from that of the other cloud albedo patterns. However, positive REOF-Frontal patterns feature a major cloud anomaly over the inland portion of the domain, probably not marine stratus and likely associated with synoptic conditions.

5. Linkage Between Cloud Albedo Variations and Surface Temperatures

[62] Several processes may affect surface temperatures, but a major candidate involves anomalous cloud cover (increased or decreased cloud albedo). Mechanisms include the reflection of solar radiation (cooling) and also the absorption and emission of infrared radiation (warming), with the former occurring during daylight hours while the later effect is most evident during the night. To investigate these effects, a series of analyses were conducted to quantify the linkage between anomalies of cloud albedo anomalies and surface temperature over California and Nevada.

5.1. Correlation of Cloud Albedo Versus Temperature

[63] In our first step in the examination of the local cloudiness versus temperature linkage, cloud albedo was correlated with daytime and nighttime temperature anomalies for June–September (JJAS). Daily T_{MIN} and T_{MAX} were obtained from available COOP stations in California and Nevada, colocated with values of daily cloud albedo taken from GOES satellite measurements. Here a daily cloud albedo was calculated by averaging over the hours 16Z–00Z (8 A.M.–4 P.M. LST).

[64] Figure 9a shows the correlation between daily values of cloud albedo and temperature for JJAS. The presence of cloud (positive cloud albedo anomaly) is associated with cooler than average daily maximum temperature, a result of the "shading" mechanism provided by cloud reflection of incoming solar radiation. Strongest correlations have negative values greater than −0.6. Largest negative correlations are found along the California coastline, indicating the effect of summertime marine stratus fluctuations in modulating daily afternoon temperature during these months. In contrast, positive anomalies of cloud albedo are associated with warmer than average daily minimum temperature (T_{MIN}), likely a result of the nighttime "blanket" effect of clouds in intercepting infrared radiation and radiating it back to the Earth's surface. Albedo versus T_{MIN} correlations have magnitudes that are generally less than 0.4, somewhat lower than those for cloud albedo versus T_{MAX}, and not as consistent spatially as the correlations for T_{MAX}. There are some locations where cloud albedo-T_{MIN} correlations are slightly negative, including the extreme southern coastline. Negative correlations along the coast may be due to advection effects, e.g., conditions when relatively strong onshore winds advect cool marine air along with marine stratus clouds over land. Also, the cloud albedo anomalies are determined from daytime cloudiness, while T_{MIN} generally occurs during the previous night.

[65] When seasonal means (JJAS) of cloud albedo and T_{MAX} are considered, similar structure to the daily T_{MAX} correlation pattern is found, in the sense that increased cloudiness is associated with lower maximum temperatures, shown in Figure 9b. It should be noted that there are only 16 years (1996–2011) of GOES satellite albedo data available, so that correlation magnitudes must exceed 0.51 to meet the 95% confidence level. These correlations indicate the importance of fluctuations in cloud cover and their shading (or not) effects on seasonal timescales. Summer season correlations with T_{MAX} along the California coast range from insignificantly small values to about −0.6. For JJAS albedo

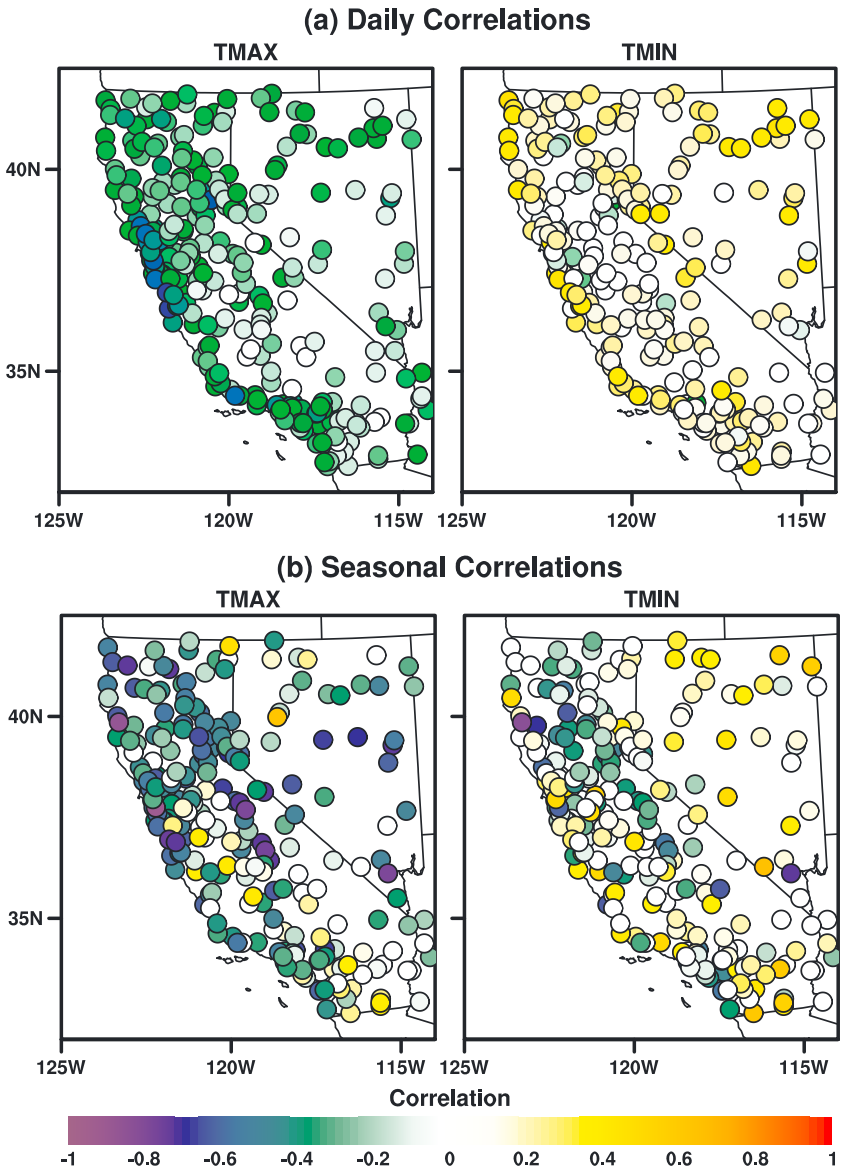

Figure 9. Local correlations of (a) daily and (b) seasonal albedo versus COOP daily T_{MIN} and T_{MAX}. Albedo average over 16–00Z for months June–September 1996–2010. The seasonal cycle was removed from each time series. Daily correlations are displayed only if significant at the 95% confidence level. All seasonal correlations are displayed; however, only those with magnitude greater than 0.51 are significant at the 95% confidence level.

versus T_{MIN}, there are a number of locations with positive correlations, but there are several sites that exhibit negative correlations, indicating the importance of other mechanisms. Seasonal mean cloud albedo versus T_{MIN} correlations display a string of relatively strong negative correlations located approximately along the Sierra Nevada range which were not obvious in the correlations of daily values but may be the result of another form of advection influence wherein cooler temperatures associate with cloudier than average conditions and vice versa are accentuated by the orographic effects.

5.2. Composite Surface Temperature Anomalies During Strong Albedo REOF Days

[66] To investigate the association of both high and low polarities of cloud albedo anomaly with surface temperature, a composite analysis was carried out. Daily T_{MAX} anomalies (long-term monthly means removed) at COOP stations were composited on JJAS days identified as strongly resembling the positive phase of each of the four leading REOF patterns using the same criteria as in section 4, namely, days with an REOF PC greater than its 90 percentile value, while the remaining three leading REOF PCs are between their 10 and 90 percentile values. The composite mean anomalous T_{MAX} for the positive phase of each REOF are shown in Figure 10a.

[67] Similarly, T_{MAX} anomalies were composited on days that strongly resembled the negative phase of each REOF pattern using the criteria that the REOF PC < 10 percentile value while the remaining three REOF PCs remain between their 10 and 90 percentile values. The negative phase

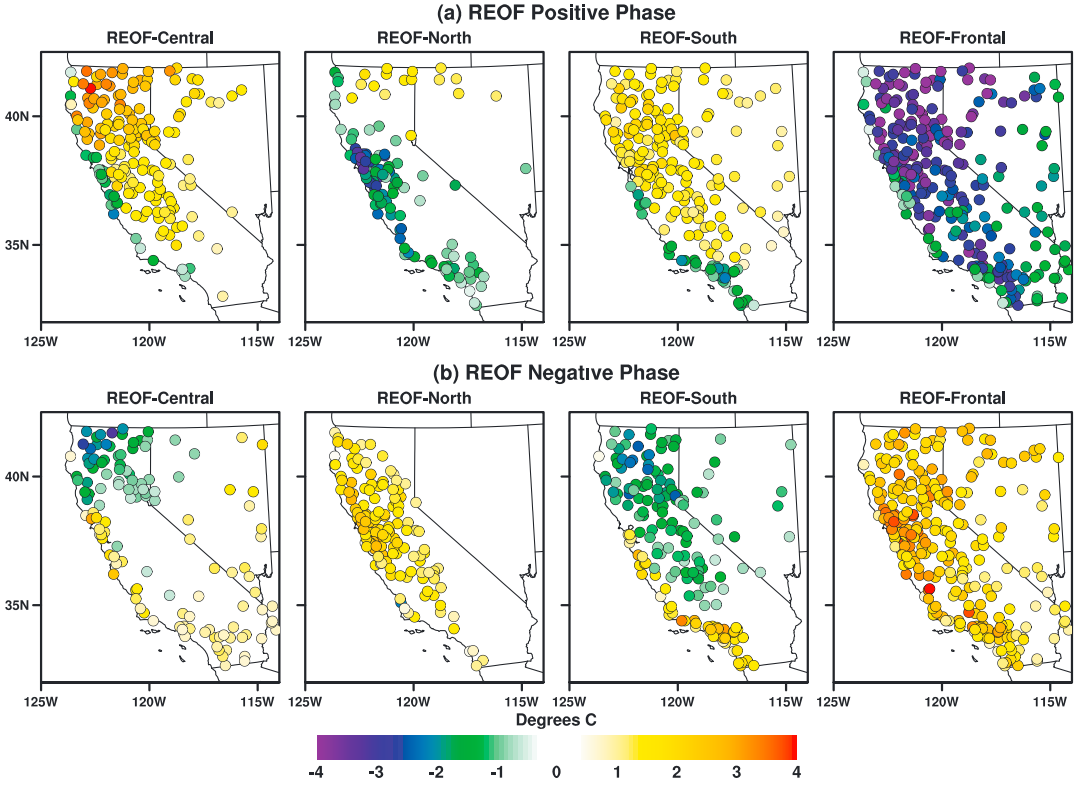

Figure 10. Composite anomalies of T_{MAX} at COOP stations for JJAS days during the (a) positive phase and (b) negative phase of each ROEF pattern shown in Figure 8. Only those composites with significance above the 95% confidence level as measured by a student *t* test are displayed.

temperature anomaly composites for each REOF are shown in Figure 10b.

[68] Daily maximum temperature anomalies during strong positive REOF-Central days show a distinct pattern with significant negative anomalies of about −1 to −2°C located mostly along the Central California coast and positive anomalies of about the same magnitude throughout the interior of California with largest positive values located in the far northern region. The positive phase of albedo pattern of REOF-Central is indicative of marine stratus along the Central California coastline, and it is clear that these clouds have a substantial cooling impact on T_{MAX} at coastal locations.

[69] During strong positive REOF-North days, negative T_{MAX} anomalies of up to −3°C are found along the coast, primarily around the San Francisco Bay region where the negative anomalies penetrate a significant distance inland even though the highest albedo values (i.e., marine stratus) end near the coastline. During strong positive REOF-North days, the inversion base height at Oakland is 155 m higher than normal (Table 2) allowing for easier inland penetration of the marine boundary layer air mass. Even though the marine stratus clouds may evaporate as they move inland, the cool marine air flowing eastward through the local mountain passes can reduce daytime temperatures in the Central Valley.

[70] The T_{MAX} anomalies during positive REOF-South days are strongly negative along the coastline southward of San Francisco reaching magnitudes of up to −2.5°C. There is also some evidence of inland penetration of these negative T_{MAX} anomalies along the extreme southern portion of the coastline. The inversion base height anomaly at San Diego is +105 m during strong positive REOF-South days which would again tend to enable the inland penetration of marine stratus clouds and cool marine air in the boundary layer. However, the distance inland is not as great as with REOF-North, due to higher local topography in this region.

[71] The T_{MAX} anomalies for these first three REOFs (Central, North, and South) all display a strong coastal-inland contrast; that is, cooler-than-normal temperatures along the coast are associated with warmer-than-normal temperatures inland (and vice versa). This is very similar to the pattern found by *Johnstone and Dawson* [2010] when they compared summer T_{MAX} anomalies at stations along the U.S. West Coast to their Northern California fog index.

[72] Temperature anomalies during positive REOF-Frontal days are much more uniform across coastal and inland locations compared to the other REOF patterns, particularly for T_{MAX}. The albedo pattern of REOF-Frontal is more typical of synoptic-scale weather systems, having a more spatially uniform impact on summertime temperature anomalies relative to REOF patterns associated with marine stratus clouds. The anomalies in this composite are relatively high, with composite cloudy REOF-Frontal days exhibiting negative anomalies between −1°C and −4°C indicating the strong influence that this pattern exerts on daytime surface temperatures over most of California and Nevada.

[73] In general, values of T_{MAX} composited over days containing the negative phase REOF patterns (Figure 10b) are nearly opposite of those composited over the positive phases (Figure 10a). In particular, positive and negative

Table 3. Multiple Linear Regression Model Results

Site	Standardized Regression Coefficients			Correlation	No. of Days
	U*ΔT	Solar	500 hPa		
Crescent City	−0.16	0.30	−0.02	0.36	1901
Arcata	−0.20	0.46	0.01	0.51	1918
Monterey	−0.42	0.44	0.06	0.66	1928
Santa Barbara	−0.07	0.45	0.06	0.48	1319
Los Angeles	−0.15	0.34	0.22	0.48	1928
San Diego	−0.18	0.36	0.28	0.54	1948

cloud cover patterns represented by the coastal cloud REOF modes 1, 2, and 3 are associated with about the same magnitude of cooling or warming of daily maximum temperatures. The main exception is REOF-Frontal where the T_{MAX}. anomaly pattern is opposite but somewhat weaker than the widespread cool temperature anomaly pattern found with the positive phase of the REOF-Frontal.

5.3. Magnitude of Radiation and Temperature Change Associated With Cloud Albedo

[74] Examination of daily mean cloud albedo versus T_{MAX} on individual days indicate that on relatively cloudy days, cooler than normal T_{MAX} usually occur. However, on days when there are little or no clouds (cloud albedo close to clear sky values), there are many cases of T_{MAX} being both cooler and warmer than normal. In other words, clear skies do not guarantee a warmer than normal day along the California coastline. For instance, in some cases onshore advection of relatively cool marine air may also increase during periods of decreased marine stratus related cloud albedo, which would counteract the warming influence expected from diminished clouds alone. In other cases, longwave radiative cooling at the tops of low-lying cloud/fog can overwhelm surface sensible and latent heating leading to a cooling throughout the boundary layer [*Koracin and Dorman*, 2001; *Koracin et al.*, 2005]. Other forms of synoptic-scale circulation variability (e.g., adiabatic heating associated with subsidence) could also impact temperature, along with cloud cover.

[75] To elaborate upon the impact individual physical processes have on T_{MAX} variability, a set of multiple linear regressions were constructed using solar attenuation, 500 hPa height, and a simple advection term as predictors of T_{MAX}. These regressions utilized measurements of temperature and wind at six coastal airports. The 500 hPa heights were taken from daily mean NCEP reanalysis data products. The solar attenuation terms were calculated using colocated GOES cloud albedo measurements. The standardized regression coefficients from these regressions provide insight into the relative importance of each process in driving T_{MAX} variability.

[76] In this model, solar attenuation (SA) was approximated using a weighted mean cloud albedo

$$SA = 1\text{-}[\sum ALB_i \times COSZ_i]/[\sum COSZ_i]$$

where COSZ is the solar zenith angle and subscript i represents the different image times during the day. The advection term (ADV) was specified as $ADV = U\times(T_{MAX} - SST)$, where SST is the sea surface temperature and was specified using the values at closest OISST grid point to each airport site. Five of the six airport locations are situated along coastline generally oriented in a north-south direction, and the U-component of wind was used to estimate the advection term. At the remaining airport (Santa Barbara), the V-component was used as the coastline is oriented in an east-west direction.

[77] It must be noted that the specification of the advection term contains the predictand, and thus, the regression is not an entirely independent diagnostic of T_{MAX}. However, the regressions are used here to estimate the contribution of each predictor to the variability of T_{MAX} and are not intended to portray a new method of predicting T_{MAX}. The main consequence is that the importance of the advection term relative to T_{MAX} variability may be artificially elevated and this should be kept in mind when interpreting these results.

[78] Table 3 contains the standardized regression coefficients at each of the six sites along with the correlation between the regressed and observed T_{MAX} time series. At every location, variability in solar attenuation is most important in estimating daily variations of T_{MAX}. Only at the Monterey airport does the advection term rival the solar attenuation in importance. It is also interesting to note that the 500 hPa predictor coefficient increases in magnitude as the site latitude decreases suggesting an increased importance for Southern California relative to Northern California.

[79] In this simple model, the solar attenuation variability was based solely on the cloud albedo. However, solar attenuation is not the only process occurring when marine stratus is present. As a result, T_{MAX} variability due to solar attenuation in this model includes contributions from both reflection of solar radiation by the clouds (attenuation) as well as a potential contribution from cloud top longwave radiative cooling. *Koracin et al.* [2005] note that when clouds are present, cloud top radiative loss can play a major role in cooling the marine layer air mass. Thus, it is expected that this longwave radiative cooling term may be on the same order of magnitude as the cooling due to the reflection of solar radiation. To adequately separate these two terms, a more sophisticated model would be required, one that includes solar and longwave radiation parameterizations.

[80] In evaluating the regression results, it is important to understand the covariability of the predictor variables. As described in Table 3, the three predictor variables are weakly correlated. Correlation between the daily time series of the advection and solar predictors varies from −0.07 to −0.23 across the six locations, and other pairings of the predictor variables exhibit similarly weak correlations. These weak correlations indicate that the three predictor variables are nearly independent, justifying the inferences drawn above. Stratus clouds appear to be the main driver of T_{MAX} variability along the coast. However, from an inspection of atmospheric circulation composited during days with no clouds (not shown), it appears that advection becomes more apparent, particularly along the Northern California coastline. Additionally, the locations used in Table 3 are situated on the immediate coastline with direct exposure to the open ocean, and the results found here may not be applicable to other sites further from the ocean but still impacted by both marine layer clouds and advection of cool marine air. Future studies should incorporate high-resolution three-dimensional modeling to provide a more thorough and complete budget analysis for locations along the immediate coast and further inland.

Table 4. Sensitivity Estimates Associated With 10% Change in Cloud Albedo[a]

Site	ΔAlbedo (%)	ΔCloud Cover (%)	ΔSolar ($W m^{-2}$)	ΔT_{MAX} (°C)
Monterey	10	20.3 ± 0.8	−99 ± 2	−1.07 ± 0.12
Santa Barbara	10	21.2 ± 0.9	−111 ± 2	−0.96 ± 0.17
Los Angeles	10	17.0 ± 0.8	−105 ± 4	−0.89 ± 0.14
San Diego	10	16.1 ± 0.7	−107 ± 3	−0.74 ± 0.12

[a]Albedo, cloud cover and downwelling solar sensitivities are based on daily mean values. Sensitivities were calculated using a regression of daily time series during months of June to September 1996–2011. The uncertainties shown in the table provide intervals with 99% accuracy based on the standard error of the regression.

[81] The above regression analysis indicates that radiative processes associated with marine stratus (cloud albedo) play a critical role in the variability of T_{MAX} at coastal locations. Another series of linear regressions were constructed to estimate the sensitivity of downwelling solar radiation (DSR) and T_{MAX} to changes in cloud albedo, and the association of surface-observed cloud cover (CLD) fluctuations to cloud albedo fluctuations. Measurements of T_{MAX} and CLD were obtained from selected coastal airport locations, while DSR measurements were obtained from the CIMIS data set. Cloud albedo was obtained from the GOES satellite data set at colocated pixels. The seasonal cycle was removed from each time series. A total of four sites (Monterey, Santa Barbara, Los Angeles, and San Diego) were selected due to the nearby proximity of an available CIMIS station to the various coastal airports used elsewhere in this study. At all four sites, the CIMIS solar station was located within 20 km of the respective airport and at an elevation within 80 m. Furthermore, each airport-CIMIS set had a similar exposure to the open ocean.

[82] At each site, time series of daily T_{MAX} and daily mean DSR and CLD were regressed onto daily mean cloud albedo and the resulting regression coefficient was used to estimate the sensitivity. The data spans the 1996–2011 period of available GOES satellite measurements and only includes the months of June through September. The sensitivities of DSR, CLD, and T_{MAX}, relative to a 10% change in cloud albedo, are shown in Table 4. To place into context a 10% change in cloud albedo, the standard deviation of daily mean cloud albedo at the four sites varies from 15 to 18% during the 1996–2011 period. It should be noted that due to the linear nature of the regressions, the magnitude of the associations is the same for either a positive or negative change in albedo and that this assumption may not necessarily be valid throughout the entire range of daily mean cloud albedo.

[83] The results are quite consistent across the four locations. An increase in daily mean cloud albedo of 10% is associated with an increase in daily mean cloud cover varying from 16 to 21% at the stations examined. As defined, albedo can vary from 0 to 100%, so the values in Table 4, if they were linearly extrapolated, would yield very large changes in cloud cover (in some cases greater than 100%), given large changes in cloud albedo. Such large variations in daily mean cloud albedo are occasionally observed, but it should be noted that these linear regressions should apply to the smaller more range of albedo and cloud cover (as well as solar and temperature) values that typically occur at each of the sites.

[84] A 10% increase in daily mean cloud albedo is associated with a decrease in incoming solar radiation of about 100 $W m^{-2}$ at the four locations included. Slightly higher values are found for the Southern California sites, as one might expect due higher solar zenith angles there due to lower latitude. The magnitude of this sensitivity is based on summer months and would be expected to decrease if winter months were considered.

[85] Perhaps the most interesting results are the sensitivities of T_{MAX} to changes in albedo which range from −0.74 to −1.07°C for a 10% increase in daily mean cloud albedo. The standard deviation of daily mean cloud albedo at these four sites varied from 15 to 18% suggesting that on daily timescales, typical temperature responses reach or exceed 1.5°C in association with day-to-day changes in cloud albedo.

6. Summary and Conclusions

[86] Surface and satellite measurements were utilized to examine the frequency of occurrence of marine stratus clouds and to determine their influence on California and Nevada surface temperatures. At 1 km horizontal resolution, the satellite albedo measurements support an examination at a scale sufficient to resolve the highly variable topographic effects in the region.

[87] The results presented here demonstrate that inversion characteristics play a major role in the variability of summertime marine stratus. Recent studies of *Lin et al.* [2009] and *Wang et al.* [2011] provide evidence that seasonal (winter-summer) differences in marine stratus are due to a deepening-decoupling mechanism rather than changes in inversion strength. These results are consistent with those obtained here, which focused on the variability of summertime marine stratus. Here, it is found that the frequency of marine stratus cloud cover in summer is closely linked with both the strength and height of the thermal inversion that caps the atmospheric marine layer (see Figure 6). The strong correlation between inversion strength and marine stratus cover agrees with the earlier results of *Klein and Hartmann* [1993] who used reanalysis products to calculate the lower tropospheric stability which was used to infer inversion strength. The present results indicate that the inversion strength is more important for marine stratus occurrence over water regions, while over coastal land areas the frequency of marine stratus is more strongly determined by the height of the inversion. The inland extent of marine stratus appears controlled by the height of the inversion and the coastal topography, and thus, the inland penetration of marine stratus is dictated by the local topography. In other words, the coastal mountains act as a barrier to further inland extent, and higher cloud heights are required to penetrate further inland.

[88] Our study did not incorporate potential interactions between inversion characteristics and aerosols, although the model and empirical testing that we conducted suggests that aerosol effects are probably incremental in modifying the association between albedo variability and temperature. As inversion strength increases and/or as inversion height lowers, one would expect the concentration of aerosols within the marine boundary layer to increase. This elevated concentration of cloud condensation nuclei could have multiple impacts including increased reflection of solar radiation, optically

thicker clouds due to smaller and more numerous cloud droplets, and increased cloud lifetimes. Cleary, additional work is needed to address the potential impacts of aerosols on marine stratus clouds.

[89] Much of the summertime cloud variation along California's coastline is linked to broad-scale North Pacific cloud patterns, dominated by relatively low-lying, but highly reflective, marine stratus clouds. The satellite albedo data revealed that variability of marine stratus is coherent on spatial scales of hundreds of kilometers along the coastal margin and is often at the eastern edge of a regional cloud pattern that extends westward and southward over the North Pacific. Topographic influences are also apparent in these patterns, whose high correlations are concentrated to the west of the first major coastal mountain front at elevations less than about 500 m. The large regional coherence exhibited by the summer cloud albedo fluctuations reinforces the premise that large-scale circulation plays a crucial role in driving this variability.

[90] Importantly, marine cloud cover (cloud albedo) variations influence surface air temperatures in California. For the most part, increased presence of cloud (higher cloud albedo) is associated with negative T_{MAX} anomalies (cooler daytime temperatures) and positive T_{MIN} anomalies (warmer nighttime temperatures). Cloud cover is not the only modifier of temperature, and undoubtedly, increased or decreased cloud albedo is often associated with other processes which themselves affect temperature. For instance, the passing of a cold front produces considerable cloud cover along the frontal boundary, but at the same time, there is advection of cold air that also impacts temperatures. However, a simple multiple regression analysis indicates that along the immediate coastline (i.e., locations within a few kilometers and with direct exposure to the open ocean), processes associated with marine stratus (i.e., reflection of solar radiation and longwave cloud top cooling) play a larger role than those due to advection or geopotential height fields in the variability of summertime values of T_{MAX}.

[91] To describe the regional-scale structure that occurs in marine cloud anomaly patterns and in their association with surface temperature anomalies, the summer cloud albedo anomaly variability was condensed into a small set of rotated empirical orthogonal functions (REOFs). Temperature composites during strong and weak occurrences of these REOFs demonstrate a strong daytime temperature sensitivity along the coastline, with enhanced cooling during days when marine stratus clouds are present. *Johnstone and Dawson* [2010] also reported a similarly strong contrast between coastal and inland correlations between T_{MAX} and their index Northern California fog frequency. Also, it is emphasized that even during summer months, cloud anomaly patterns not associated with marine stratus are present (REOF-Frontal) that exhibit strong impacts on surface temperatures throughout California and Nevada.

[92] Overall, the results suggest that characterizing and predicting cloud cover variations would be useful in predicting temperature a few days in advance or, if skill is available, at seasons in advance. The results here strongly emphasize the importance of marine clouds in inhibiting warmer than average daytime temperatures along the coastal margin. Conversely, when these regularly occurring clouds are absent, there is a tendency for anomalously warm coastal daytime temperatures. Extreme warm temperatures can occur when synoptic conditions lower the inversion base height to the point where the formation of marine stratus is reduced or eliminated. *Gershunov et al*.'s [2009] study of California heat waves focused on the severe (in terms of human mortality) heat wave of July 2006, which was noteworthy in having little or no marine stratus along the California coastline. The highest mortality rates during this event were in the coastal regions where the strongest positive T_{MAX} anomalies occurred. Results presented here reinforce those proposed in *Gershunov et al*. [2009], demonstrating how anomalously warm coastal temperatures are permitted when marine clouds are absent.

[93] **Acknowledgments.** The authors sincerely appreciate the input from three anonymous reviewers whose insightful comments and suggestions greatly improved the manuscript. This work was supported by the California Energy Commission through the California Climate Change Center and by the NOAA Regional Integrated Sciences and Assessments (RISA) Program through the California-Nevada Applications Program (CNAP). The GOES satellite measurements were obtained from NOAA's Comprehensive Large Array-data Stewardship System (CLASS) website at http://www.nsof.class.noaa.gov. The ISCCP D2 data were obtained from the International Satellite Cloud Climatology Project web site http://isccp.giss.nass.gov maintained by the ISCCP research group at the NASA Goddard Institute for Space Studies, New York, NY. The airport cloud and temperature observations were obtained from the Global Surface Hourly database at http://www.ncdc.noaa.gov operated by the NOAA National Climatic Data Center (NCDC). The Cooperative Observer Network daily temperature records were also obtained from NCDC.3.

References

Alfaro, E. J., A. Gershunov, and D. Cayan (2006), Prediction of summer maximum and minimum temperature over the Central and Western United States: The roles of soil moisture and sea surface temperature, *J. Climate*, *19*, 1,407–1,421.

Blaskovic, M., R. Davies, and J. B. Snider (1991), Diurnal variation of marine stratocumulus over San Nicolas Island during July 1987, *Mon. Weather Rev.*, *119*, 1,469–1,478.

Bretherton, C. S., and M. C. Wyant (1997), Moisture transport, lower-tropospheric stability, and decoupling of cloud-topped boundary layers, *J. Atmos. Sci.*, *54*, 148–167.

Briegleb, B. P. (1992), Delta-Eddington approximation for solar-radiation in the NCAR community climate model, *J. Geophys. Res.*, *97*, 7,603–7,612.

d'Almeida, G. A., P. Koepke, and E. P. Shettle (Eds) (1991), *Atmospheric Aerosols: Global Climatology and Radiative Characteristics, A*, Deepak Publishing, Hampton, VA.

Duynkerke, P. G., and P. Hignett (1993), Simulation of a diurnal variation in a stratocumulus-capped marine boundary layer during FIRE, *Mon. Weather Rev.*, *121*, 3,291–3,300.

Filonczuk, M., D. Cayan, and L. Riddle (1995), Visibility of marine fog along the California coast, *Scripps Institution of Oceanography Report*, 95-2, 102 pp.

Fischer, D. T., C. J. Still, and A. P. Williams (2008), Significance of summer fog and overcast for drought stress and ecological functioning of coastal California endemic plant species, *J. Biogeography*, *36*, 783–799, doi:10.1111/j.1365-2699.2008.02025.x.

Gershunov, A., D. Cayan, and S. Iacobellis (2009), The great 2006 heat wave over California and Nevada: Signal of an increasing trend, *J. Climate*, *22*, 6,181–6,203.

Hartmann, D. L., M. E. Ockert-Bell, and M. L. Michelsen (1992), The effect of cloud type on Earth's energy balance: Global analysis, *J. Climate*, *5*, 1,281–1,304.

Hess, M., P. Koepke, and I. Schult (1998), Optical properties of aerosols and clouds: The software package OPAC, *Bull. Am. Meteorol. Soc.*, *79*, 831–844.

Horel, J. D. (1981), A rotated principal component analysis of the interannual variability of the Northern Hemisphere 500 mb height field, *Mon. Weather Rev.*, *109*, 2,080–2,092.

Iacobellis, S. F., J. R. Norris, M. Kanamitsu, M. Tyree, and D. R. Cayan (2009), Climate variability and California low-level temperature inversions. *California Climate Change Center*, Publication # CEC-500-2009-020-F. Available online at: http://www.energy.ca.gov/2009publications/CEC-500-2009-020/CEC-500-2009-020-F.PDF.

Intergovernmental Panel on Climate Change (2007), *Intergovernmental Panel on Climate Change Fourth Assessment Report: Climate Change 2007 (AR4)*, Cambridge University Press, Cambridge, United Kingdom.

Johnstone, J. A., and T. E. Dawson (2010), Climatic context and ecological implications of summer fog decline in the coast redwood region, *Proc. Nat. Acad. Sci.*, *107*, 4,533–4,538.

Kaiser, H. F. (1958), The varimax criterion for analytic rotation in factor analysis, *Psychometrika*, *23*, 187–200.

Kalnay, E., et al. (1996), The NCEP/NCAR 40-year reanalysis project, *Bull. Am. Meteorol. Soc.*, *77*, 437–470.

Klein, S. A., and D. L. Hartmann (1993), The seasonal cycle of low stratiform clouds, *J. Climate*, *6*, 1,587–1,606.

Koracin, D., and C. E. Dorman (2001), Marine atmospheric boundary layer divergence and clouds along California in June 1996, *Mon. Weather Rev.*, *129*, 2,040–2,056.

Koracin, D., J. Businger, C. Dorman, and J. Lewis (2005), Formation, evolution, and dissipation of coastal sea fog, *Boundary Layer Meteorology*, *117*, 447–478.

Lebassi, B., J. Gonzalez, D. Fabris, E. Maurer, N. Miller, C. Milesi, P. Switzer, and R. Bornstein (2009), Observed 1970–2005 cooling of summer daytime temperature in coastal California, *J. Climate*, *22*, 3,558–3,573.

Leipper, D. F. (1994), Fog on the United States West Coast: A review, *Bull. Am. Meteorol. Soc.*, *75*, 229–240.

Lilly, D. K. (1968), Models of cloud-topped mixed layers under strong inversions, *Q. J. Roy. Meteorol. Soc.*, *94*, 292–309.

Lin, W., M. Zhang, and N. G. Loeb (2009), Seasonal variation of the physical properties of marine boundary layer clouds off the California coast, *J. Climate*, *22*, 2,624–2,637.

Madej, M. A., C. Currens, V. Ozaki, J. Yee, and D. G. Anderson (2006), Assessing possible thermal rearing restrictions for juvenile coho salmon (oncorhynchus kisutch) through thermal infrared imaging and in-stream monitoring, Redwood Creek, California, *Can. J. Fish. Aquat. Sci.*, *63*, 1,384–1,396, doi:10.1139/F06-043.

Mathiesen, P., J. M. Brown, and J. Kleissl (2013), Geostrophic wind dependent probabilistic irradiance forecasts for coastal California, *IEEE Trans. on Sustainable Energy*, *4*, 510–518, doi:10.1109/TSTE.2012.2200704.

Namias, J. (1978), Persistence of U.S. seasonal temperatures up to one year, *Mon. Weather Rev.*, *106*, 1,557–1,567.

National Climatic Data Center (2003), Data documentation for data set 3200 (DSI-3200): Surface land daily cooperative summary of the day. National Climatic Data Center, Asheville, NC, 36 pp. (available online at http://www.ncdc.noaa.gov/pub/data/documentlibrary/tddco/td3200.pdf).

Petterssen, S. (1938), On the causes and forecasting of the California fog, *Bull. Am. Meteorol. Soc.*, *19*, 49–55.

Pilie, R. J., E. J. Mack, C. W. Rogers, U. Katz, and W. C. Kocmond (1979), The formation of marine fog and the development of fog-stratus systems along the California coast, *J. Appl. Meteorol.*, *18*, 1,275–1,286.

Randall, D. A., J. A. Coakley, C. W. Fairall, R. A. Kropfli, and D. H. Lenschow (1984), Outlook for research on marine subtropical stratocumulus clouds, *Bull. Am. Meteorol. Soc.*, *65*, 1,290–1,301.

Reynolds, R. W., N. A. Rayner, T. M. Smith, D. C. Stokes, and W. Wang (2002), An improved in situ and satellite SST analysis for climate, *J. Climate*, *15*, 1,609–1,625.

Richman, M. B. (1986), Rotation of principal components, *J. Climatol.*, *6*, 293–335.

Rossow, W. B., and R. A. Schiffer (1991), ISCCP cloud data products, *Bull. Am. Meteorol. Soc.*, *72*, 2–20.

Rossow, W. B., A. W. Walker, D. E. Beuschel, and M. D. Roiter (1996), International Satellite Cloud Climatology Project (ISCCP) documentation of new cloud datasets, *World Meteorological Organization*, WMO/TD-No. 737, 115 pp. (available online at: isccp.giss.nasa.gov/pub/documents/d-doc.pdf).

Rozendaal, M. A., C. B. Leovy, and S. A. Klein (1995), An observational study of the diurnal cycle of marine stratiform cloud, *J. Climate*, *8*, 1,795–1,809.

Schwartz, B. E., and M. Govett (1992), A hydrostatically consistent North American radiosonde data base at the Forecast Systems Laboratory, 1946–present, NOAA Technical Memorandum ERL FSL-4. Available online at http://raob.fsl.noaa.gov/intl/radiosonde.pdf.

Stephens, G. L. (1978), Radiation profiles in extended water clouds: 2. Parameterization schemes, *J. Atmos. Sci.*, *35*, 2,123–2,132.

Van den Dool, H. M., and J. L. Nap (1985), Short and long range air temperature forecasts near an ocean, *Mon. Weather Rev.*, *113*, 878–887.

Wang, L., Y. Wang, A. Lauer, and S.-P. Xie (2011), Simulation of seasonal variation of marine boundary layer clouds over the Eastern Pacific with a regional climate model, *J. Climate*, *24*, 3,190–3,210, doi:10.1175/2010JCLI3935.1.

Williams, A. P., C. J. Still, D. T. Fischer, and S. W. Leavitt (2008), The influence of summertime fog and overcast clouds on the growth of a coastal California pine: A tree-ring study, *Oecologia*, *156*, 601–611, doi:10.1007/s00442-008-1025-y.

Wood, R. (2012), Stratocumulus clouds, *Mon. Weather Rev.*, *140*, 2,373–2,423, doi:10.1175/MWR-D-11-00121.1.

Wood, R., and C. S. Bretherton (2006), On the relationship between stratiform low cloud cover and lower-tropospheric stability, *J. Climate*, *19*, 6,425–6,432.

World Meteorological Organization (1983), World Climate Programme, Report of the Experts Meeting on Aerosols and Their Climatic Effects, *WCP-55*, Geneva.

Wu, X., and F. Sun (2005), Post-launch calibration of GOES imager visible channel using MODIS, *Proc. SPIE* 5882, Earth Observing Systems X, 58820N (September 7, 2005); doi:10.1117/12.615401.